NRC Research Press

ARTICLE

Three-dimensional levee and floodwall underseepage

Navid H. Jafari, Timothy D. Stark, Aaron L. Leopold, and Scott M. Merry

Abstract: Levee and floodwall seepage models based on two-dimensional (2D) conditions can underpredict landside vertical hydraulic gradients and uplift pressures due to excavations and convex bends. The Sherman Island levee system is used to calibrate a three-dimensional (3D) seepage model to evaluate the effect of finite landside excavations and convex levee bends on landside seepage. The model shows that a 3D analysis is required for a landside excavation with an aspect ratio (length to width) less than 1*L*:1.5*W*. For drainage canals and ditches that parallel a levee or floodwall and are wider than 15 m, gradients at the excavation center are essentially equal to 2D vertical gradients but greater than 2D gradients near the excavation sidewalls. The Sherman Island calibrated seepage model also confirms concave bends diverge seepage and yield lower vertical gradients than 2D models. Varying the degree of levee curvature (ω = 45°–100°) indicates that sharper convex bends (ω = 100°; axisymmetric radius, 150 m) cause vertical gradients that can be about 150% greater than 2D analyses.

Key words: two-dimensional (2D) seepage, three-dimensional (3D) seepage, levee, floodwall, concave, convex, excavation, axisymmetric, transient analysis, hydraulic gradient, uplift.

Résumé : Les modèles d'infiltration bidimensionnels (2D) appliqués aux digues et murs de protection contre les crues peuvent sous-estimer les gradients hydrauliques dans le sol et la sous-pression hydrostatique causés par des excavations et des courbures convexes. Le dispositif de digues de l'île Sherman sert à calibrer un modèle d'infiltration tridimensionnel (3D) qui permet d'évaluer les effets d'excavations creusées dans le sol et des courbures convexes de digues sur l'infiltration d'eau dans le sol. Le modèle montre qu'il est nécessaire de réaliser une analyse 3D dans le cas d'une excavation dont le rapport de forme (longueur sur largeur) est inférieur à (1.*L*)/(1,5.*l*). Dans le cas de canaux et de fossés de drainage qui sont parallèles à une digue ou à un mur de protection contre les crues et dont la largeur est supérieure à 15 m, les gradients au centre de l'excavation sont pratiquement égaux aux gradients verticaux 2D, mais supérieurs aux gradients 2D situés à proximité des parois de l'excavation. Le modèle d'infiltration calibré et utilisé à l'île Sherman confirme également que les courbures concaves font diverger les flux d'infiltration et produisent des gradients verticaux inférieurs à ceux obtenus dans les modèles 2D. En faisant varier le degré de courbure de la digue (ω = 45°–100°), on montre que les fortes courbures convexes (ω = 100°; rayon axisymétrique, 150 m) génèrent des gradients verticaux qui peuvent être supérieurs d'environ 150 % à ceux obtenus au moyen d'analyses 2D. [Traduit par la Rédaction]

Mots-clés : modèle d'infiltration bidimensionnel (2D), modèle d'infiltration tridimensionnel (3D), digue, mur de protection contre les crues, concave, convexe, excavation, axisymétrique, analyse transitoire, gradient hydraulique, sous-pression.

Introduction

Two-dimensional (2D) seepage models can underpredict landside hydraulic gradients under landside excavations and convex levee bend conditions (Money 2006; Cobos-Roa and Bea 2008; Ahmed and Bazaraa 2009; Benjasupattananan and Meehan 2012). For example, Money (2006) reports computed three-dimensional (3D) vertical hydraulic gradients that are ~45% and ~120% greater than 2D computed hydraulic gradients for infinite and finite landside excavations, respectively. Ahmed and Bazaraa (2009) show that neglecting seepage flow through excavation sidewalls can lead to errors in computing the landside uplift pressures and exit gradients. Benjasupattananan and Meehan (2012) and Merry and Du (2015) report higher 3D uplift pressures and hydraulic gradients at the landside toe for convex levee sections compared to 2D models. While 2D models underpredict hydraulic gradients for convex bends, concave bends diverge underseepage, resulting in 2D models that overpredict gradients. An industry guidance document (URS 2013) accounts for 3D effects by recommending an increase in average exit vertical gradient by 20%–30% for 60° levee angles.

The state of practice for examining levee and floodwall seepage is 2D finite element analyses (FEA) and (or) analytical solutions proposed in the U.S. Army Corps of Engineers (USACE) design manuals EM 1110-2-1901 and EM 1110-2-1913 (USACE 1993, 2000). The 2D FEA calculates uplift pressures and flow assuming levee geometry, soil stratigraphy, boundary conditions, and excavations are infinitely wide. However, urban levees and floodwalls are constructed to accommodate natural river meanders, and landside excavations are often present. Examples of limited extent landside excavations include borrow pits, building foundations, agricultural storage silos and tanks, residential swimming pools, burrowing animals, trees, utilities, conduits, pipelines, drainage canals, and culverts.

This study uses a segment of Sherman Island levees to field calibrate a seepage model and then perform a parametric analysis using the calibrated model to investigate the effects of 3D landside excavations and levee bends on landside hydraulic gradients. For 3D effects on landside excavations, the excavation width is varied to identify when a 3D analysis is warranted. Floodside excavations are not discussed herein because the maximum landside hydraulic gradients can be estimated using a 2D cross section

Received 17 August 2014. Accepted 18 June 2015.

N.H. Jafari and T.D. Stark. University of Illinois at Urbana-Champaign, 205 N. Mathews Ave., Urbana, IL 61801, USA.
A.L. Leopold. Shannon & Wilson Inc., 1321 Bannock St., Denver, CO 80204, USA.
S.M. Merry. University of the Pacific, 3601 Pacific Avenue, Stockton, CA 95211, USA.
Corresponding author: Navid H. Jafari (e-mail: njafari2@illinois.edu).

that bisects the floodside excavation. Therefore, floodside excavations can be conservatively modeled using a 2D seepage analysis, whereas landside excavations require a 3D analysis (Stark and Jafari 2015). The levee bend analysis investigates the 3D vertical gradients along a curved segment of Sherman Island. A calibrated parametric analysis is performed to evaluate the effect of convex and concave meanders on 3D landside vertical gradients, and a methodology is proposed to simulate 3D bends with 2D axisymmetric models.

Sherman Island

The Sacramento – San Joaquin Delta (referred to herein as Delta) is located at the confluence of the Sacramento and San Joaquin Rivers in Northern California. The Delta is important to California's economy and infrastructure, including a source of water supply for about 25 million Californians, a source of irrigation for over 7 million acres (2.83 million hectares) of agricultural land, and an extensive infrastructure of state and local roads, railroads, pipelines, and shipping ports (CALFED 2000). A levee network protects the many islands in the Delta and directs water to San Francisco Bay. Combined with subsiding interiors and high flood levels, levees and their foundations are vulnerable to seepage and seepage-induced failures. In particular, subsidence is a major concern on Sherman Island because a lower landside elevation increases the hydraulic gradient from floodside to landside. From 1930 to the early 1980s, over 50 Delta islands or tracts flooded primarily due to levee foundation instability (Prokopovitch 1985). Significant consequences occur after a levee breach, such as in 2004 when the Lower and Upper Jones Tract flooded, resulting in economic impacts of greater than $100 million (California DWR 2005). Therefore, assessing seepage-induced levee performance on flood protection infrastructure is important to public health, commercial activities, and environmental safety of the Delta and Sherman Island.

Sherman Island lies at the western limit of the Delta where the Sacramento and San Joaquin rivers converge and is bordered to the northeast by Threemile Slough (see Fig. 1*a*; USDA (2014)). The island is located northeast of the city of Antioch, California, and is within the jurisdiction of Sacramento County. Sherman Island is currently protected by approximately 29 km of perimeter levees (Hanson 2009). The levees were originally constructed in the 1860s' over organic soils and have been enlarged periodically as the foundation soils subsided. Approximately 15 km of Sherman Island levees are constructed to federal standards and supervised by the USACE, while the remaining 14 km of levees are nonproject levees (maintained by the local levee district). Subsidence and substandard levee protection have resulted in major levee breaches that have inundated Sherman Island in 1904, 1906, 1909, and 1969.

In 1969, the levee segment on the San Joaquin River between levee Stations 520 and 525 (see Fig. 1*b*; USDA (2014)) failed, and the high-velocity flow from the levee breach eroded the island interior and created a scour hole about 6.5 m deep (see scour lake in Fig. 1*b*). Since 1969, seepage and stability problems have plagued the southern levees (south of Antioch Bridge to Station 545). Numerous piezometers, inclinometers, and settlement plates are being used to monitor levee performance between Stations 520 and 545 (see rectangle in Fig. 1*a*) to help prevent another breach (Hanson 2009). Borings from previous studies were utilized to develop a subsurface profile at cross section A–A′ in Fig. 1*b*, and a nearby piezometer was used to calibrate the 2D and 3D seepage models developed herein. These seepage models permitted an investigation of landside excavations and levee curvature on underseepage and landside vertical gradients and uplift pressures.

Levee profile and soil properties

The subsurface profile shown in Fig. 2 was developed using borings B-1, B-2, and B-3 from Hanson (2009). The boring locations shown in Fig. 1*b* were drilled as part of the levee improvements along landside of Sherman Island from approximately Stations 520 to 545. Borings B-1 and B-2 are located in the free field, i.e., beyond the landside levee toe, while B-3 is located at the landside toe. Borings B-1, B-2, and B-3 were drilled prior to the 2009 remedial measures. The aerial view in Fig. 1*b* was photographed in 2012 after construction of a landside stability berm began; therefore, borings B-1 and B-2 appear at the landside toe, and B-3 appears located at the levee crest after remediation.

The levee foundation is composed of a range of coarse-grained sediments, including gravels and loose clean sands, and silty sands. Thus, the profile in Fig. 2 starts at depth with a fine sand stratum below elevation (el.) –15 m NAVD88 (North American Vertical Datum of 1988). Above the sand is a layer of silty clay, locally known as Bay Mud, deposited as the sea level rose following the last ice age. The clay stratum is about 3.1 m thick and overlain by

Fig. 1. Aerial photographs: (*a*) Sherman Island (white box shows location of aerial photograph in *b*); (*b*) close-up showing location of cross section A–A′ and nearby instrumentation (USDA (2014), photos from 2012 [http://datagateway.nrcs.usda.gov/]).

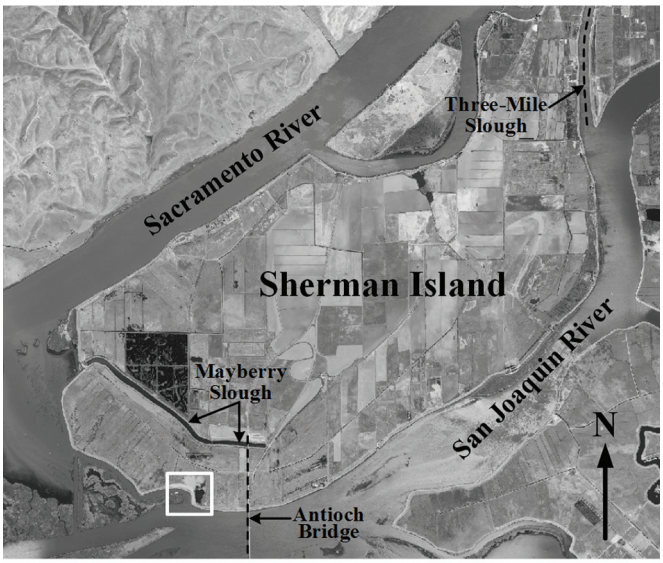

(a)

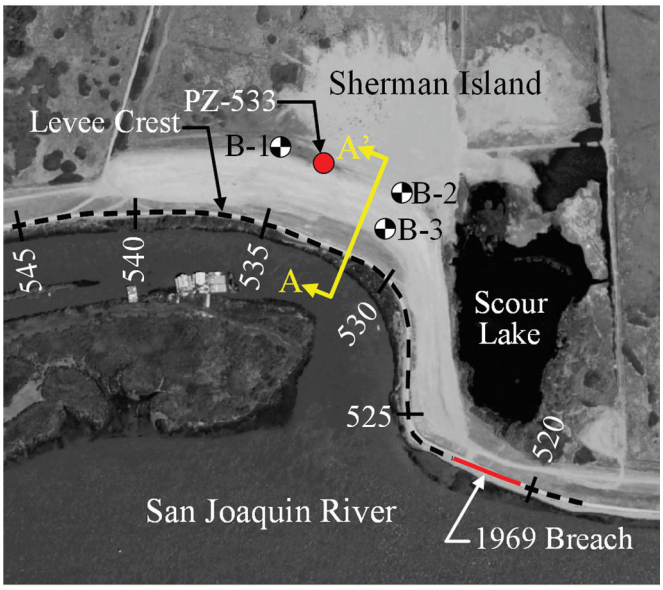

(b)

Fig. 2. Levee cross section A–A′ of Sherman Island at Station 532. h_t, total head; Q, flow rate.

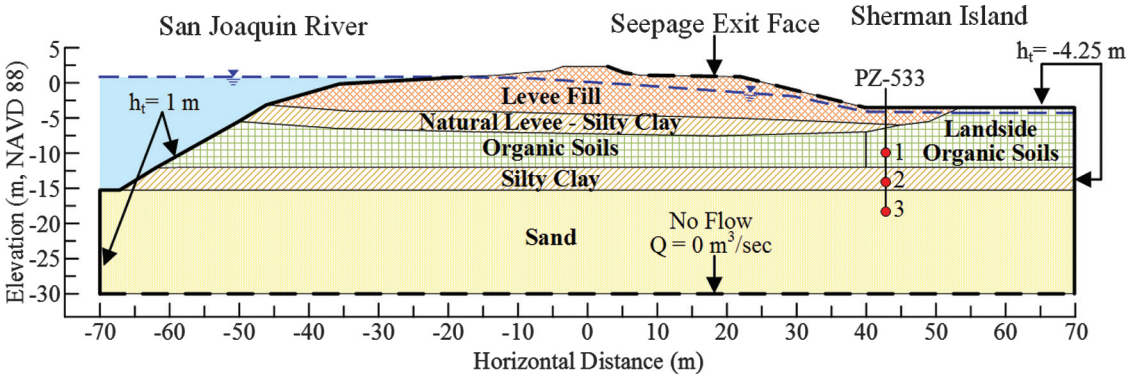

organic soils that extend to the ground surface. Shelmon and Begg (1975) report sea level rise in the past 7000 years created tule marshes that covered most of the Delta. The repeated burial of the tules and other vegetation growing in the marshes formed approximately 8 m of highly organic soils at cross section A–A′. The highly organic soils are not classified as peat because the organic content (ASTM D2974 (ASTM 2014)) and classification defined in ASTM D4427 (ASTM 2013) are not available to confirm sufficient organics for peat classification, i.e., greater than 75% organics.

The Sherman Island levee embankment is composed of dredged loose to medium sand and silt. Weight of the levee embankment has caused settlement of the organic soil layer and hence a decrease in horizontal hydraulic conductivity. In addition, the levee fill overlies natural levees of the San Joaquin River, which are represented by a layer of silty clay between the organic soil and levee fill. This natural levee material, known locally as overbank deposits, is found to be of limited lateral extent, grading into the thick organic soil stratum beneath the levee berms.

Water levels are maintained 0.6–1.5 m below land surface by an extensive network of drainage ditches. Foott et al. (1992) report an artesian condition in the sand substratum, causing upward seepage through the clays and organic soils. The foundation seepage is typically drained off, collected, and pumped out of the island via a series of levee toe drainage ditches flowing to a pumping station (see toe ditch in Fig. 2).

Table 1 summarizes index properties and engineering parameters used in the seepage analyses. Due to the weight of levee fill, the natural water content (w_o) of the organic soils under the levee ranges from 116% to 265%, while the landside organic soils have natural water contents from 224% to 408% (Weber 1969; Foott et al. 1992). The resulting organic soil saturated unit weight (11.6 kN/m^3) is greater than the landside organic soils (10.5 kN/m^3) and is in agreement with unit weights reported in Mesri and Ajlouni (2007). Available hydraulic conductivity tests are limited for the levee embankment, silty clay, and sand materials shown in Fig. 2. As a result, estimates of saturated horizontal hydraulic conductivity (k_h) for these soils in Table 1 were made using the Guidance Document for Geotechnical Analyses by URS (2013). The value of k_h for the organic soils is evaluated using Weber (1969), Mesri and Ajlouni (2007), and Mesri et al. (1997) and the appropriate average effective vertical stress (σ'_{va}). Weber (1969) utilized piezometer data to estimate k_h of the organic soils in the Delta using an inverse analysis and found k_h ranges from 1×10^{-7} to 1×10^{-4} cm/s for $\sigma'_{va} \leq 550$ kPa. The σ'_{va} of organic soils under the levee and landside toe is about 190 and 45 kPa, respectively, based on the cross section in Fig. 2. This σ'_{va} correlates to a k_h of about 3×10^{-5} and 3×10^{-4} cm/s for organic soils under the levee and landside, respectively. The anisotropy ratio, i.e., ratio of horizontal to vertical hydraulic conductivity (k_h/k_v), is 3–5 for surficial peats and about 10 for buried peat deposits (Mesri and Ajlouni 2007). Thus, the values of k_h/k_v chosen for Sherman Island organic soils are 10 and 3 for organic soils at the landside toe and under the levee, respectively. Based on URS (2013), the anisotropy ratio is assumed to be 4 for levee fill and 10 for the sand and natural silty clays. These values of saturated k_h and k_h/k_v ratios are consistent with those used for the certification of the nearby Natomas levees (Merry and Du 2015). Because this study is focused on underseepage during steady-state conditions, the unsaturated soil properties are not modeled for the levee embankment fill and landside organic clay.

Table 1. Soil index properties and hydraulic parameters for cross section A–A′ in Fig. 2.

Soil type	Soil classification (ASTM 2011)	γ_{sat} (kN/m^3)	w_o (%)	k_h (cm/s)	k_h/k_v
Levee fill	ML or SM	17.7	8–13	1×10^{-3}	4
Organic soil under levee	OL or OH	11.6	116–265	3×10^{-5}	10
Landside organic soil	OL or OH	10.5	224–408	3×10^{-4}	3
Silty clay	CL–ML	16.7	49–78	1×10^{-6}	10
Sand	SM or SP	19.5	25–35	1×10^{-2}	10

Note: CL, low-plasticity clay; ML, silt; OH, organic clay; OL, organic silt; SM, silty sand; SP, poorly graded sand; γ_{sat}, saturated unit weight.

Calibration of 2D seepage model

The 2D finite element program SEEP/W by Geo-Slope (2007) was used to estimate the phreatic surface through the levee fill and calibrate pore-water pressures in the substratum using available Sherman Island piezometer data. SEEP/W is a general seepage analysis program formulated to model saturated and unsaturated transient flow through soil and excess pore-water pressure dissipation estimated from a stress–deformation analysis within porous materials. Piezometer PZ-533 was installed in 2008 at Station 533 to monitor pore-water pressures during landside stability improvements (Hanson 2009). The initial pore-water pressures prior to construction of the stability berm were used to calibrate the 2D and 3D seepage models.

The initial floodside steady-state boundary condition is a total head (h_t) of el. +1 m NAVD88 and is consistent with canal water levels measured at the Antioch gage station. The "seepage exit face" option was selected from the levee crest to landside levee toe (40 m from levee centerline in Fig. 2) because the phreatic surface on the landside levee slope is unknown. The boundary condition from landside levee toe to the right-hand side (RHS) of the finite element mesh is assumed to be 0.75 m below the ground surface (el. –4.25 m NAVD88). The left-hand side (LHS) vertical boundary is specified as the steady-state river stage (el. +1 m NAVD88) because the sand stratum is hydraulically connected to the San Joaquin River (Foott et al. 1992). In addition, with the sand stratum hydraulically connected to the San Joaquin River, the results are insensitive to the vertical floodside boundary condition (Du and Merry 2014). The bottom boundary condition is defined as an impervious boundary to represent the low hydraulic conductivity clay under-

Table 2. Calibration of Sherman Island seepage model at steady-state conditions.

Piezometer	Depth (m)	Soil layer	Measured h_t (m)	SEEP/W h_t (m)
1	–9.6	Organic soil	–4.0	–4.2
2	–14.2	Silty clay	–3.0	–3.1
3	–18.8	Sand	–2.7	–2.8

lying the sand stratum. Figure 2 shows the soil profile and boundary conditions used in the calibration model.

The cross section in Fig. 2 is calibrated using data from PZ-533, which is located 43 m landside from the levee centerline and at ground surface el. –3.5 m NAVD88. Three piezometers shown in Fig. 2 were installed at el. –9.6 m (PZ-533-1), –14.2 m (PZ-533-2), and –18.8 m (PZ-533 = 3) in PZ-533 (Hanson 2009). The total heads in Table 2 were recorded prior to construction of the improvement activities. The total heads of –3 and –2.7 m measured by PZ-533-2 and PZ-533-3, respectively, indicate artesian conditions exist in the sand layer, which confirms the hydraulic connection between the San Joaquin River and sand stratum. A comparison of PZ-533 response and the SEEP/W results at steady state is shown in Table 2. The SEEP/W model slightly overestimates the pore-water pressures but is in close agreement with measured values. The phreatic surface computed in SEEP/W is shown in Fig. 2. Based on the initial pore-water conditions and phreatic surface, the 2D calibrated model was used to perform 3D simulations of landside excavations and levee bends.

Effect of landside excavations

The effect of floodside and landside excavations came to the forefront in litigation related to the floodwall breaches along the Inner Harbor Navigation Canal (IHNC) and was the impetus for this 3D study (Stark and Jafari 2015). Prior to Hurricane Katrina, the USACE contracted for the demolition and environmental cleanup of the East Bank Industrial Area (EBIA) in the IHNC to allow for widening of the shipping canal. The EBIA had a long history of industrial use and contamination (WGI 2005), as well as the presence of buried structures and foundations that could interfere with dredging of a bypass channel in the IHNC. Thus, the removal of contaminated soil and buried structures resulted in many floodside excavations along the IHNC floodwalls. If these excavations were backfilled with high hydraulic conductivity soils and penetrated to depths below the tip of the floodwall sheet pile, floodside underseepage could have been facilitated.

Stark and Jafari (2015) performed 3D seepage analyses to understand the IHNC floodwall breaches and found the maximum 3D landside vertical gradients correspond to a 2D cross section through the floodside excavation. In contrast, the 3D seepage analyses show that landside excavations cause 3D gradients to increase because of inward seepage from the excavation sidewalls. With landside drainage ditches, borrow pits, building foundations, residential swimming pools, and tree stumps located near levees, landside excavations were investigated to evaluate 3D flow on landside hydraulic gradients and provide recommendations on when a 3D seepage analysis is warranted.

Formation of 3D model

The 3D Sherman Island seepage model in Fig. 3 was developed using the software package RS^3 (Rocscience 2014) to compare the effect of finite landside excavations with the calibrated 2D SEEP/W model in Fig. 2. The soil profile, hydraulic properties, and levee geometry are identical between the two models (SEEP/W and RS^3). The 3D model geometry is constructed by extruding the 2D profile "into the page" in Fig. 2. The 3D model uses three extruded slices to model the excavation, with the center slice modified to include an open excavation. The outer two slices duplicate Fig. 2 and are 50 m wide to control end effects (see Fig. 3). The excavation width is varied by widening the center slice. The landside toe ditch is replaced with the landside excavation. The boundary conditions shown in Fig. 3 include a seepage exit face applied to the inside surfaces of the excavation because water can seep into the excavation during flood conditions. This boundary condition is applied in open excavations, e.g., during construction of building foundations, swimming pools, and underground utilities. The floodside and LHS vertical boundary conditions are assumed a maximum river stage of el. +1.8 m NAVD88. The boundary condition from the landside levee toe to the RHS of the finite element mesh is zero pressure head (h_p). The RHS vertical boundary is modeled as a total head boundary (h_t = el. –3.5 m or at the ground surface) to represent the landside groundwater conditions. The boundary condition along the bottom of the seepage model remains a no-flow boundary. Figure 4 shows the 2D flow field and total head contours at a river stage of el. +1.8 m. The total head contours decrease from +1.8 m at the floodside to –6 m at the bottom of the excavation. The contours in the sand stratum are horizontal, indicating head loss through the stratum is minimal. The total head contour of el. –6 m at the bottom of the excavation corresponds to hydraulic gradients close to 0.4.

Landside excavation parametric results

The multiple excavation widths used to compute the vertical hydraulic gradients at the center and edge of a landside excavation are shown in Fig. 5. Points 1 and 2 are positioned along the centerline of the landside excavation, and points 3 and 4 are located at the excavation edge (sidewall). At widths of 2 m, high gradients observed in the center of the excavation are attributed to inward seepage from the sidewalls. For excavations less than 3 m, the gradients measured at points 1 and 3 as well as points 2 and 4 are equal because of the short distance between the edge and center of the excavation. The lower gradients at points 2 and 4 as compared to points 1 and 3, respectively, are attributed to increased seepage length to the middle of the excavation. As the excavation width increases, gradients converge to 2D results (obtained from the cross section that bisects the excavation) and the effect of inward seepage is less at points 1 and 2.

For this analysis, points 1 and 2 approach 2D equivalent gradients when the excavation width is at least 15 m. This width corresponds to an excavation aspect ratio (length to width, *L*:*W*) of 1*L*:1.5*W* and is considered the threshold when vertical gradients in the excavation center are not influenced by 3D seepage. Vertical gradients are always higher at points 3 and 4 compared to the excavation center because of converging flow along the excavation sidewalls. For example, points 3 and 4 approach a constant hydraulic gradient of 0.66 and 0.44, respectively, at 10 m width. For widths >20 m, the vertical gradients at points 3 and 4 are about 150% and 190% greater than points 1 and 2, respectively. As a result, seepage-induced failures (heave or sands boils) can develop near the excavation sidewalls, as well as in the center for narrow excavations, having an aspect ratio of 1*L*:1.5*W* or less.

Figure 6 shows total head contours at steady-state flood condition with increasing excavation widths. The total head contours are el. –6.5 m at the excavation floor and el. –3.5 m on the landside surface. The concentrated total head contours for the 5 m excavation in Fig. 6*b* indicate greater change in total head and higher vertical exit gradients within the excavation. As the excavation width is increased in Figs. 6*b*–6*e*, the total head contours in front of the excavation straighten and the contours are spaced farther apart at the excavation sidewalls, thus arriving at 2D conditions. Total head contours in Fig. 6 corroborate the results in Fig. 5 by showing 3D seepage effects are limited for excavation widths greater than 15 m and the excavation sidewall is the critical zone to evaluate vertical hydraulic gradients and uplift pressures.

Fig. 3. 3D soil stratigraphy, boundary conditions, and landside excavation used in RS³.

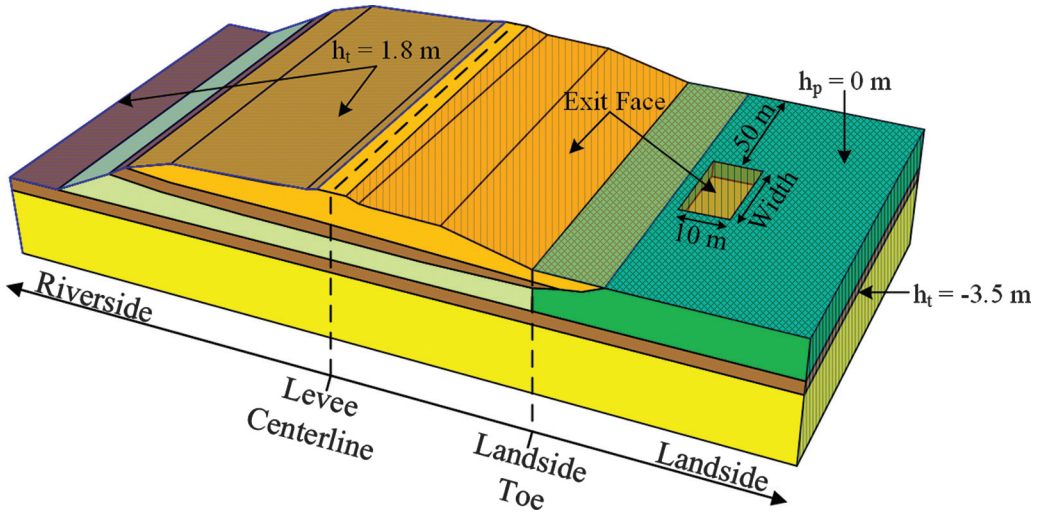

Fig. 4. 2D flow field and total head contours through excavation.

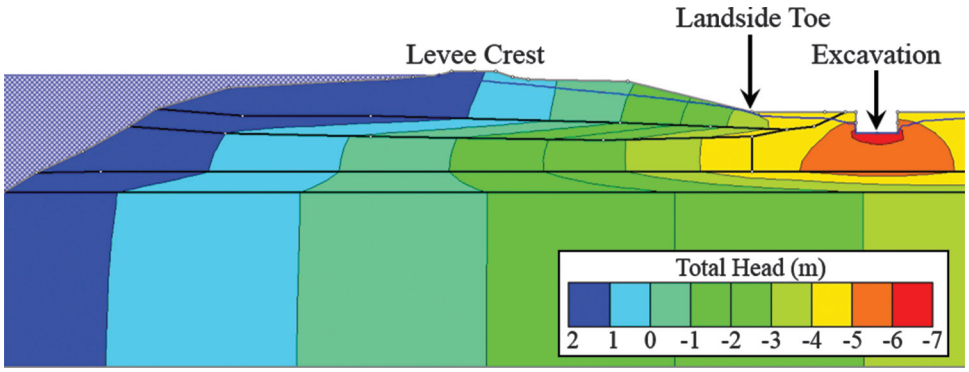

Fig. 5. Changes in vertical hydraulic gradient with increasing landside excavation width are compared with 2D seepage analyses through excavation.

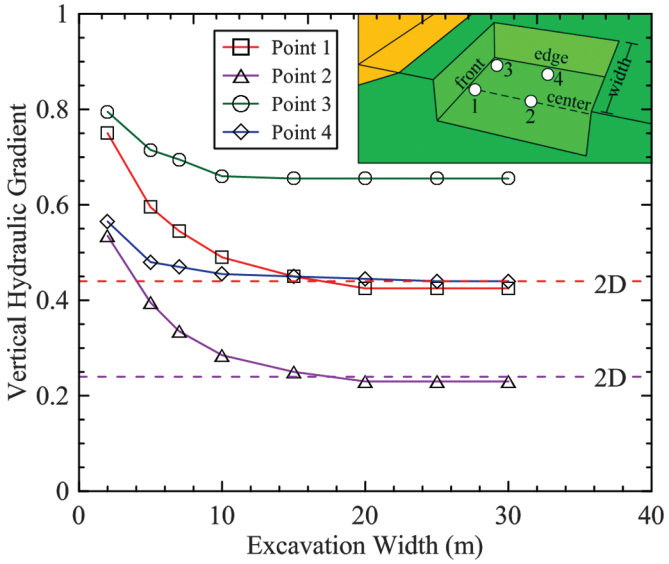

The analyses in Figs. 5 and 6 correspond to open excavations, which may be present for a temporary period. Closed excavations consist of an impermeable structure or lining, e.g., buried culverts, building foundations, and swimming pools, and can be prone to heave or sand boils around the excavation if excessive uplift pressures develop. Increases in uplift pressure can be facilitated by the structure not allowing migration of the hydraulic pressures and acting as a dam. Thus, it is necessary to compare the average uplift pressure in the excavation and the applied overburden stress. The uplift pressures were computed using RS³ by applying a no-flow boundary condition in the excavation bottom and sidewalls. This boundary condition yields an average 3D uplift pressure of 31 kPa. By estimating an overburden pressure due to the building or construction, the factor of safety against uplift for the building foundation can be computed.

The parametric analyses indicate that a 3D analysis should be used for a finite landside excavation with an aspect ratio less than 1*L*:1.5*W*. Because this aspect ratio is site specific and can depend on material hydraulic conductivity, soil profile, and excavation geometry and location from the landside toe, this example is used to simply illustrate the importance of 3D flow in landside excavations. Narrow excavations, e.g., trenches, pipelines, conduits, animal burrows, and tree stumps, are likely to impact floodwall or levee performance because vertical gradients rapidly increase below widths of 5 m. For cases such as drainage canals and toe ditches that run parallel to the levee and are greater than 15 m wide, the gradients at the center of the excavation are approximately equal to 2D vertical gradients, and therefore a 2D analysis can be performed.

Fig. 6. 3D total head contours for (*a*) model and landside excavation widths of (*b*) 5 m, (*c*) 10 m, (*d*) 20 m, and (*e*) 30 m.

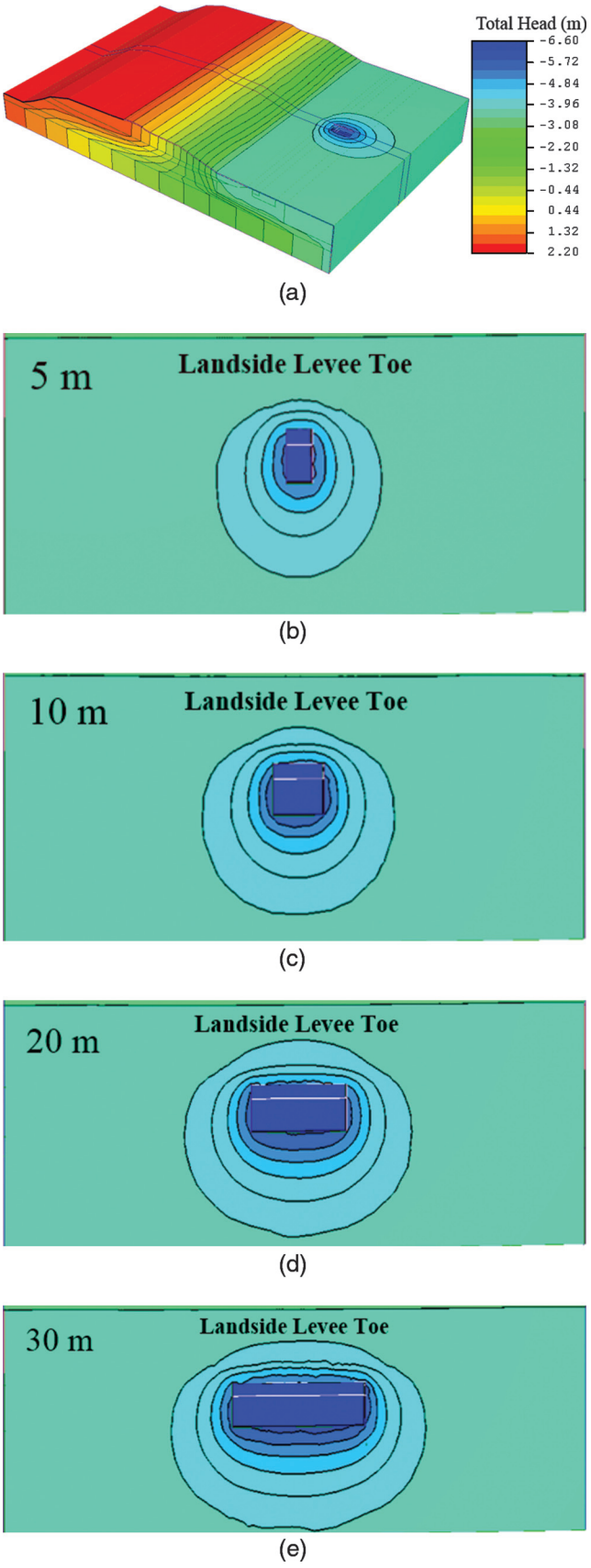

Unfortunately, Money (2006) reports that 3D vertical gradients can be 145% greater than 2D models for infinitely long landside excavations, e.g., toe drainage ditches. These results are in disagreement with Fig. 5, which illustrates long excavations, i.e., widths >15 m, approach 2D vertical gradients. The reason for this overprediction is not clear, but the authors recreated the Money (2006) 2D model and found that decreasing the mesh element size from 1.5 m (5 ft) to 0.15 m (0.5 ft) increased 2D hydraulic gradients closer to the 3D values. In other words, it appears the 2D values in Money (2006) are too low by about 145% possibly due to mesh size issues.

Effect of levee bends

The course of a river is classified as straight, meandering, or braided based on its sinuosity and other characteristics of the channel (Langbein and Leopold 1966; Morisawa 1985). Straight channels are slightly sinuous, and the occurrence of bends is random. Meandering channels can be highly convoluted or merely sinuous but maintain a single thread in curves having definite geometric shape. Braided channels are those with multiple streams separated by bars or islands, e.g., Sherman Island in Fig. 1*a*. Similar to the levees bordering Sherman Island in Fig. 1*b*, levee systems are constructed parallel to rivers and other water surfaces. As a result, levees consist of concave and convex bends, and these 3D effects can facilitate underseepage and instability.

Formation of 3D model

The 3D seepage model used to evaluate the effect of levee curvature was created in ModelMuse and input into MODFLOW 2005 (Harbaugh 2005). MODFLOW is a 3D groundwater model that can simulate steady and transient flow in an irregularly shaped flow system and with a combination of confined and unconfined aquifer layers. The surface and river topography for Sherman Island Stations 526–534 were developed from U.S. Geological Survey (USGS) geographic information system (GIS) data (Coons et al. 2008). The GIS data are imported into ModelMuse, and inverse distance square interpolation is used to create the 0.5 m surface contours in Fig. 7. MODLFOW uses the finite-difference solving method and discretizes the model into a grid. The grid spacing is defined in the *x*–*y* plane and then the model is constructed in the *z* direction by selecting a number of cells for each soil layer (see Fig. 7 for coordinate system). The grid consists of an equal spacing of 1 m by 1 m (each cell is 1 m^2) in the *x*–*y* plane, and 20 cells are specified in the *z* direction. The cells become denser in the *z* direction where changes in soil properties occur between layers.

Soil layers and material properties are defined by drawing polygons in the *x*–*z* plane and extruding these polygons in the *y* plane. Figure 8 shows the cross section that was used in MODFLOW. The subsurface profile in Fig. 8 is simplified compared to Fig. 2 because sufficient data are not present to accurately address spatial variations in soil stratigraphy and material properties. As a result, the soil layers in Fig. 8 are modeled as layers of constant thickness and elevation. For example, the organic soil layer is modeled with a thickness of 8.5 m and is located between el. –12 and –3.5 m NAVD88.

The boundary conditions used in MODFLOW are depicted in Figs. 7 and 8. To create the hydraulic connection (LHS h_t = 1.8 m), a line is specified along the center of the river and extruded in the *z* plane. A constant river stage of el. +1.8 m NAVD88 is applied to the cells that intersect this plane. For the floodside surface total head condition, a polygon is extended in the *x*–*y* plane at el. +1.8 m NAVD88 and is applied to only the surface cells. The landside surface boundary is assumed to be "free draining", which corresponds to the SEEP/W seepage exit face boundary. For the vertical landside boundary condition, a line parallel to the levee crest is drawn 70 m from the landside toe. The line is extruded in the vertical direction to create a plane. The vertical plane is set to a total head value of –3.5 m, i.e., the ground surface elevation. As a result, the LHS and RHS boundary conditions are applied so that

Fig. 7. ModelMuse surface geometry created from GIS topographical elevations and 3D boundary conditions.

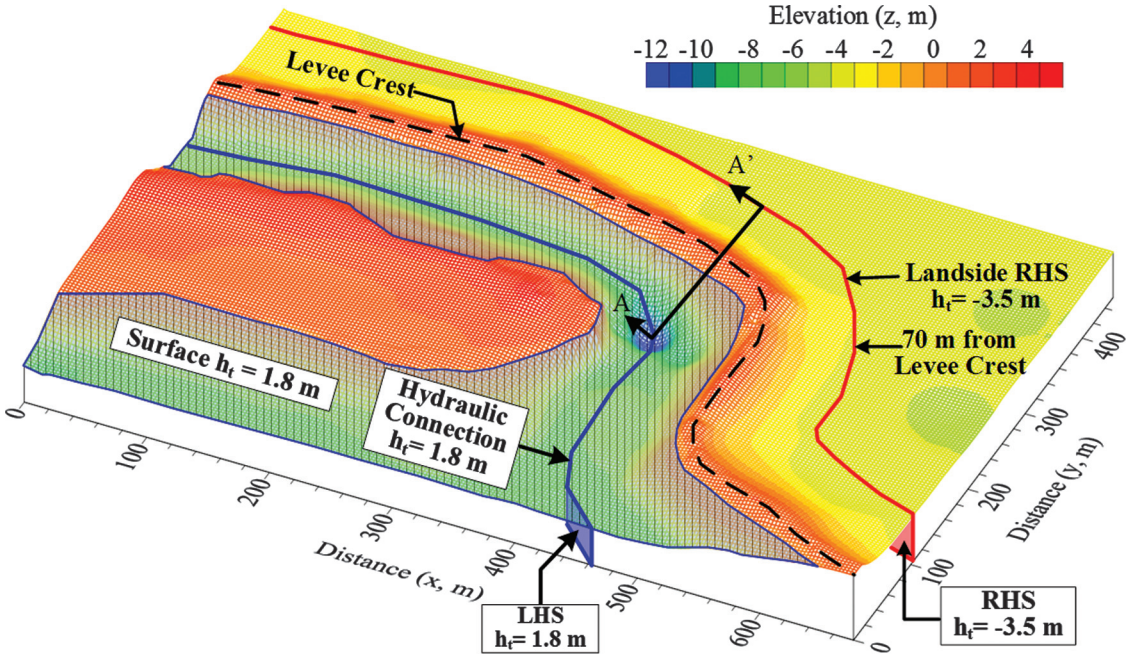

Fig. 8. Cross section A–A′ and boundary conditions of 3D model in MODFLOW at Station 532.

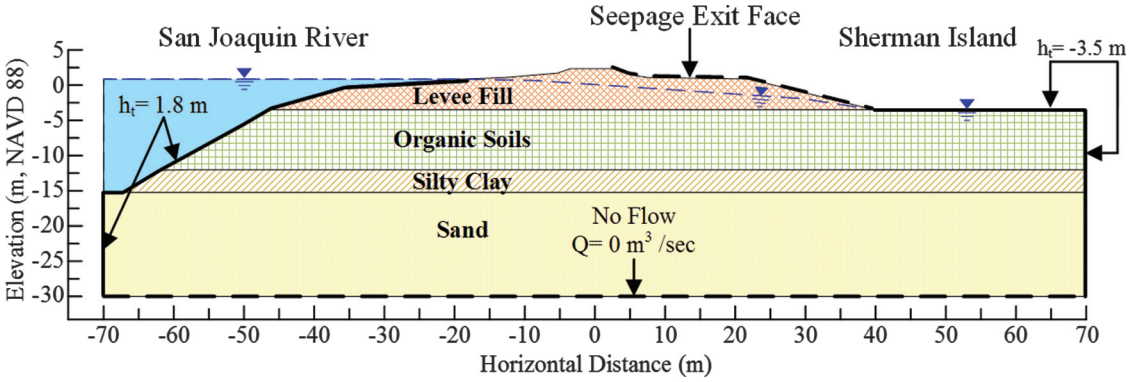

the model horizontal extents (–70–70 m) in Fig. 8 are the same as Fig. 2.

Sherman Island results

Figure 9 shows the MODFLOW hydraulic gradients at the landside toe from Stations 526 to 534. The aerial photograph in Fig. 1*b* shows the location of Stations 526–534 along the San Joaquin River. The vertical gradient is 0.36 at Station 526 and linearly decreases to a minimum of about 0.20 at Station 528. The vertical gradient remains in the range of 0.20–0.24 from Stations 528+00 to 532+50, and increases to 0.30 at Station 534. The low gradients between Stations 528 and 532 correspond to the concave curvature of the Sherman Island levee (see Fig. 1*b*). The corresponding 2D gradient at Station 532 in SEEP/W for the cross section in Fig. 8 is 0.32. This gradient comparison indicates that 2D results overpredict vertical gradients by about 160% (0.2–0.32) for concave bends. Hydraulic gradients approach the 2D model at Station 534 because the levee is transitioning to a straight segment. In addition, 3D vertical gradients are greater than 2D vertical gradients at Station 526+50 because of the convex curve at Station 525. Therefore, the 3D results in Fig. 9 highlight the important role of levee curvature and the necessity to evaluate 3D hydraulic gradients

Fig. 9. 3D vertical hydraulic gradients located between levee Stations 526 and 534.

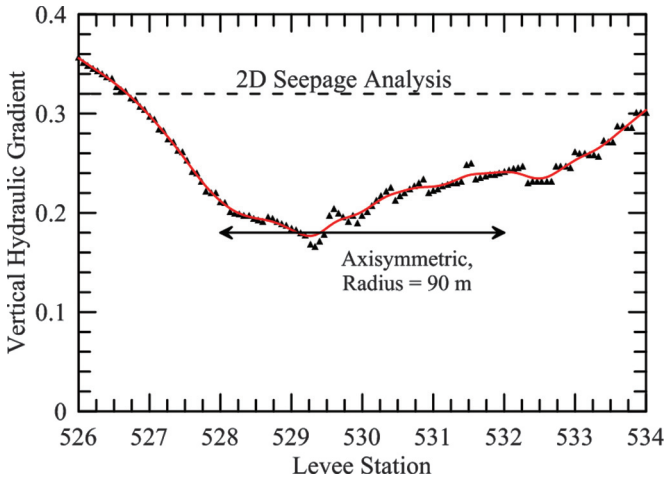

Fig. 10. Example of SGC for $\omega = 110°$: (*a*) channel direction; (*b*) levee meander.

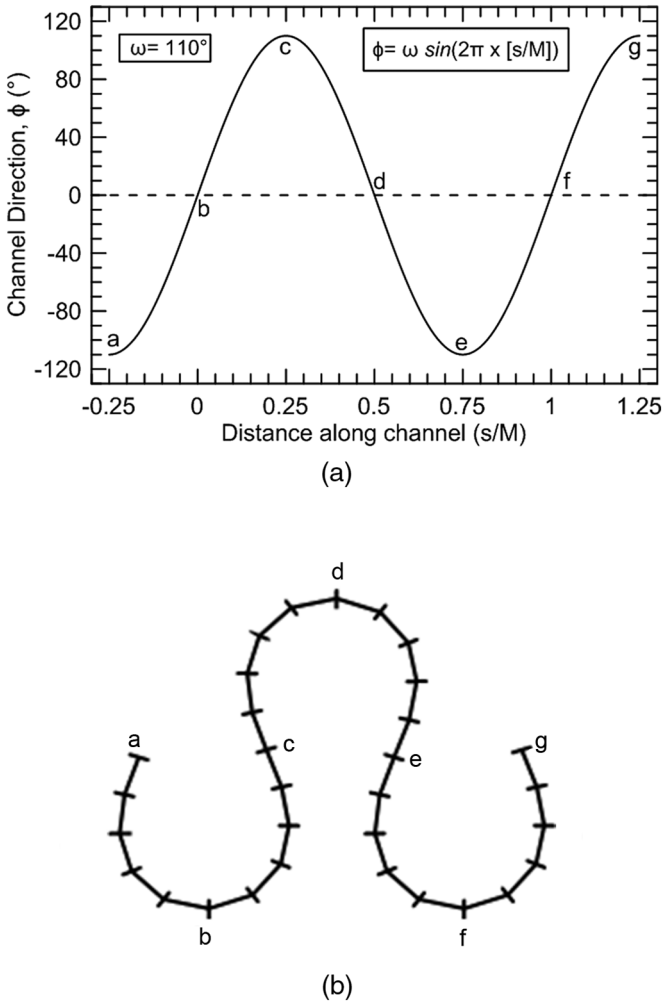

Fig. 11. Various SGC simulating levee bends used in 3D parametric analyses: (*a*) $\omega = 45°$; (*b*) $\omega = 60°$; (*c*) $\omega = 90°$; (*d*) $\omega = 100°$.

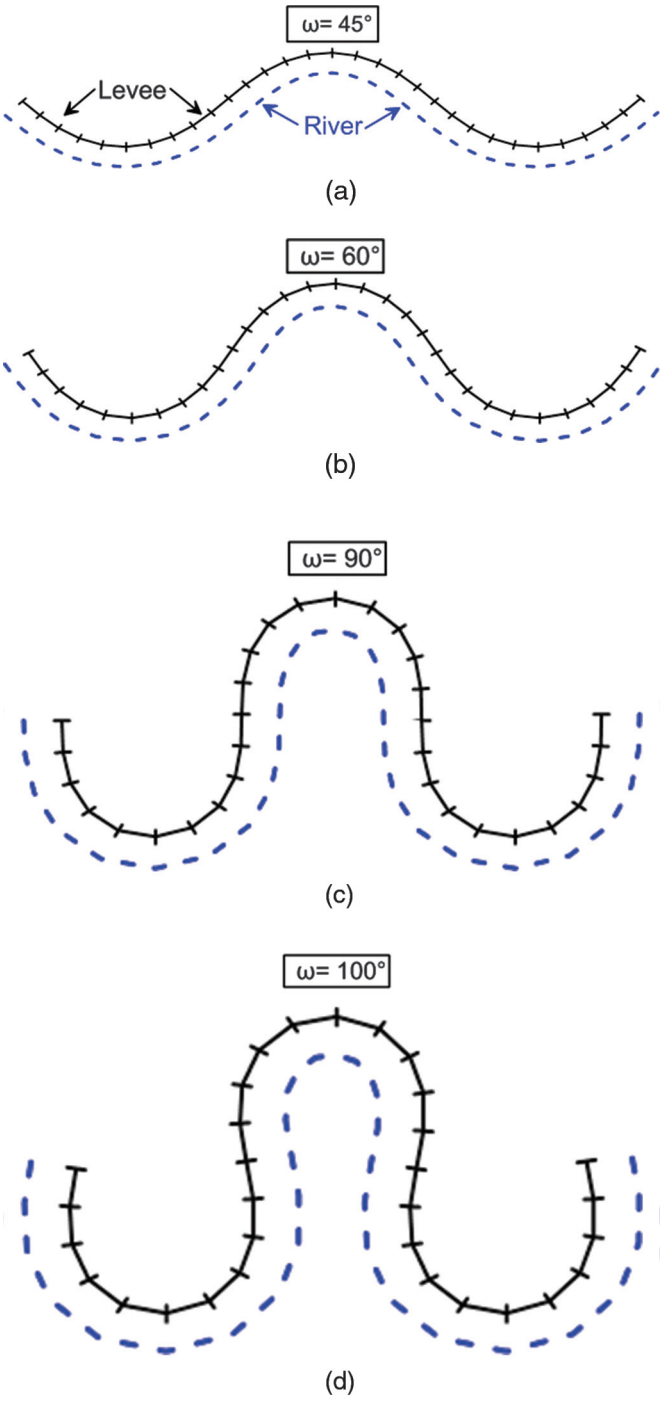

with methods that go beyond 2D plane strain analyses, especially where convex bends are present.

Levee bend parametric analyses

Typical river meanders do not follow common geometric curves, therefore Langbein and Leopold (1966) describe meander loops as sine-generated curves (SGC). They reason the SGC curve is statistically probable because it requires the smallest variation in change of direction and hence represents the least amount of work by the river. The SGC is recognized as descriptive of a self-forming river planform geometry (Yalin 1992; Soar and Thorne 2001). The planimetric geometry described in Langbein and Leopold (1966) of river meanders is defined as

$$\phi = \omega \sin\left(\frac{s}{M} 2\pi\right) \quad (1)$$

where ϕ equals the meander direction (angle) at location s, ω is the maximum angle the meander takes to the general direction of levee, and M is the levee length of a meander. Equation (1) defines the angular direction of the curve at various meander distances. Figure 10 shows an example of the SGC using $\omega = 110°$ in eq. (1) to calculate the channel direction (ϕ). The value of ϕ is zero at the curve apex (see points b, d, and f in Figs. 10*a* and 10*b*). The value of ϕ is equal to ω at points of inflection, which are illustrated in Fig. 10*b* at points c and e. Therefore, the angle ω is the critical parameter for specifying the amount of sinuosity or horseshoe looping and ranges from zero for a straight levee to a maximum of 125°.

The SGC is adopted herein for characterizing levee bends because levees are constructed parallel to rivers. Figure 11 shows four SGC examples of levee meanders used in the parametric analyses. As the value of ω increases, the meander changes from a sinuous curve to a horseshoe shape. The river in Fig. 11 is depicted at a constant distance perpendicular to the levee. In this parametric analysis, the various levee meander profiles in Fig. 11 are modeled in MODFLOW (see Fig. 12 for $\omega = 60°$) and are used to evaluate the effect of levee curvature on 3D vertical gradients. The soil

Fig. 12. MODLFOW topography and boundary conditions used in levee curvature parametric analyses (Fig. 9 shows 2D cross section of soil profile).

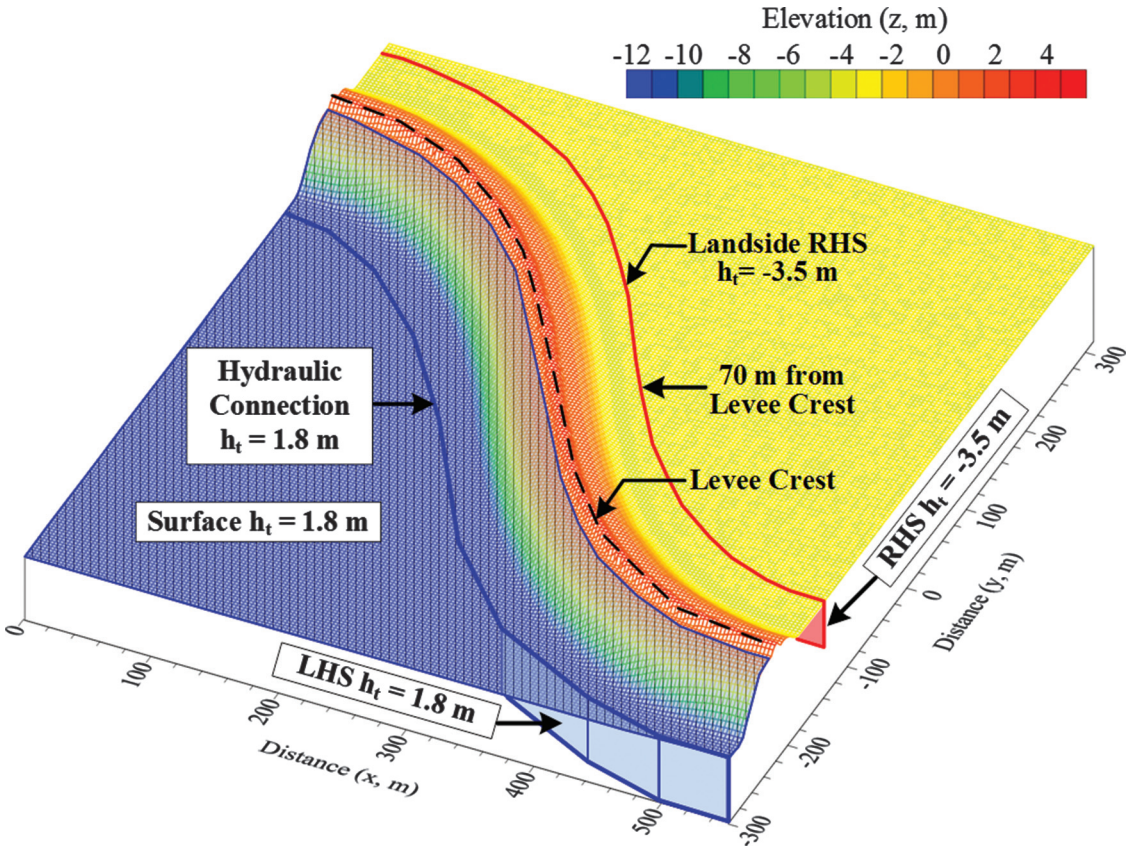

profile and boundary conditions are illustrated in Figs. 8 and 12, and are applied in the same procedure as the MODFLOW Sherman Island 3D analysis. Because the levee meanders in Fig. 11 are symmetric, the segment between points b and d in Fig. 10*b* is modeled and shown in Fig. 12.

Parametric results

Figure 13 shows the landside levee toe hydraulic gradients for ω values of 45°, 60°, 90°, and 100°. The gradients for all ω values are equal to the 2D gradient of 0.32 at the inflection point, where the levee segment is straight between convex and concave bends. From distance 0 m (the inflection point) to 200 m (maximum convex curvature), the vertical gradients increase to a maximum value at the convex bend apex. For ω of 90° and 100°, the maximum gradients approach 0.5 while gradients of about 0.4 correspond to ω of 45° and 60°. Thus, increasing convex curvature results in vertical gradients that are about 150% greater than the 2D model. Concave bends yield hydraulic gradients in the range of 0.22–0.28 for all ω values, which are slightly less than 2D values. Figure 13 shows that the concave gradients at maximum curvature are within a narrower range (~0.06) than convex bends (~0.12). Because the levee changes to a horseshoe shape at ω of 100° (see Fig. 11*d*), this causes the floodside boundary to enclose the landside area. As a result, the 3D underseepage concentrates flow into the landside and gradients increase more rapidly. In contrast, concave bends divert seepage away from the landside so 3D effects between ω values are less pronounced. As the levee curvature transitions from ω of 60° to 90°, the convex gradients in Fig. 13 increase from ~0.39 to ~0.48. The increase in gradient of ~25% indicates a critical ω value and levee curvature between 60° and 90° where 3D effects can contribute more to landside vertical hydraulic gradients.

Figure 14 presents the landside toe vertical gradients along the levee meander (distance from 0 to ±200 m) as a function of radius. The meander distance from 0 to ±200 m is divided into 200 nodes. A radius is determined for each node (n) by inscribing a circle that is tangent to the node n and neighboring nodes ($n+1$ and $n-1$). In Fig. 15, the radii for ω of 45°, 60°, 90°, and 100° corresponding to the levee bend apex (see Fig. 10 point b) are 305, 220, 155, and 150 m, respectively. These radii represent the maximum curvature of meanders in Fig. 11 and hence signify the critical section for evaluating vertical hydraulic gradients. Figure 14 shows the vertical gradients converge to the 2D value of 0.32 when radii are above ~1000 m, or close to the inflection point. The vertical gradients in Fig. 14 are also independent of ω because the 3D flow has been transformed from Cartesian to radial coordinates, i.e., equivalent radii correspond to equal gradients.

Axisymmetric model and results

The steady-state equation for radial flow is

$$(2)\qquad \frac{k_r}{r}\frac{\partial h_t}{\partial r} + k_r\frac{\partial^2 h_t}{\partial r^2} + k_z\frac{\partial^2 h_t}{\partial z^2} = 0$$

where k_r and k_z are the hydraulic conductivities in the radial and vertical directions, respectively; r is the radius; and h_t is the total head (Connor and Brebbia 1976; Bennett et al. 1990; Reddy 1993; Rao 1999). Because steady-state flow is present in eq. (2) and the hydraulic conductivity values remain constant, the rate of change

Fig. 13. Results of 3D levee curvature analyses and comparison with values from 2D seepage analyses.

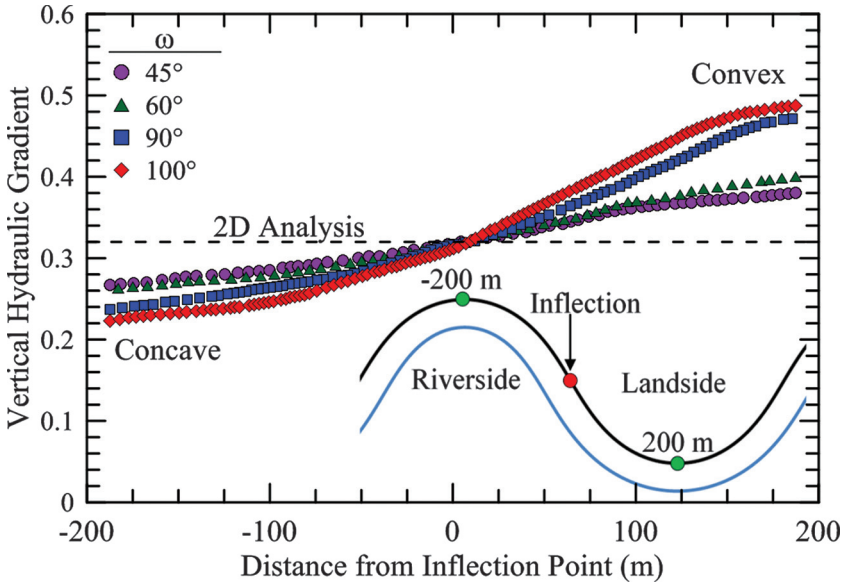

Fig. 14. Comparison of 3D MODFLOW parametric analysis and axisymmetric model.

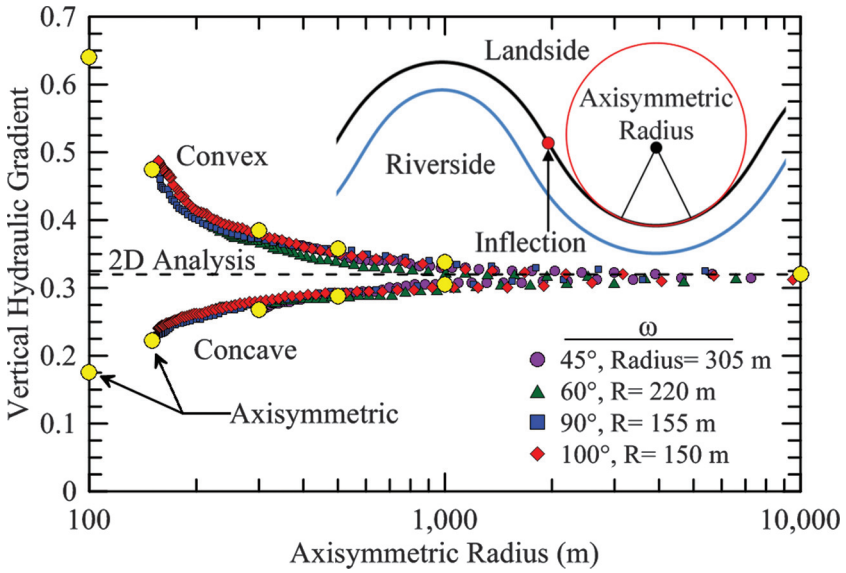

in total head in the radial direction ($\partial h_t/\partial r$) must increase as radius decreases. To compensate for the progressive decrease in flow area (radius is decreasing), $\partial h_t/\partial r$ must increase towards the axis of symmetry, which is similar to a drawdown curve. In a concave bend where the axis of symmetry is located in the floodside, decreasing the radius causes more head loss to occur before reaching the landside toe. In contrast, decreasing the radius of a convex bend generates higher total heads and vertical gradients near the landside toe before the sharp drawdown curve at the axis of symmetry.

Merry and Du (2015) use an axisymmetric model to compare hydraulic gradients of plane strain and curved levees, but do not investigate whether or not an axisymmetric analysis can accurately model 3D levee meanders. The Sherman Island cross section in Fig. 8 and levee meander parametric analysis in Fig. 11 provide an opportunity to use 3D MODLFOW results to evaluate the accuracy of axisymmetric models in curved levee seepage analyses. An axisymmetric formulation involves a 2D cross section where the origin of the horizontal axis is taken as the axis of symmetry. In an axisymmetric analysis, a concave levee bend rotates with respect to the floodside while a convex bend rotates with respect to the landside. An assumption in axisymmetric modeling is the LHS, RHS, levee centerline, and levee landside toe should all lie within concentric circles. For example, if a levee radius of 300 m describes a concave bend and the levee toe is located 20 m from the levee centerline, the radius at the levee toe is assumed to be 320 m. SEEP/W also rotates the model about the origin, so the model cannot transverse into the negative x axis.

When developing a plane strain 2D analysis, the LHS of the model is extended to the river or hydraulic boundary centerline. The RHS boundary is recommended to be extended sufficiently such that the boundary condition does not affect pore-water pressures near the levee. Several trial analyses are required to locate the RHS boundary. An axisymmetric model can be developed once the limits (RHS and LHS) of the plane strain model are selected. The axisymmetric radius describing the levee meander must be outside of the horizontal extent of the plane strain model. For example, Fig. 15 shows the calibrated Sherman Island cross section in

Fig. 15. Axisymmetric model of Sherman Island.

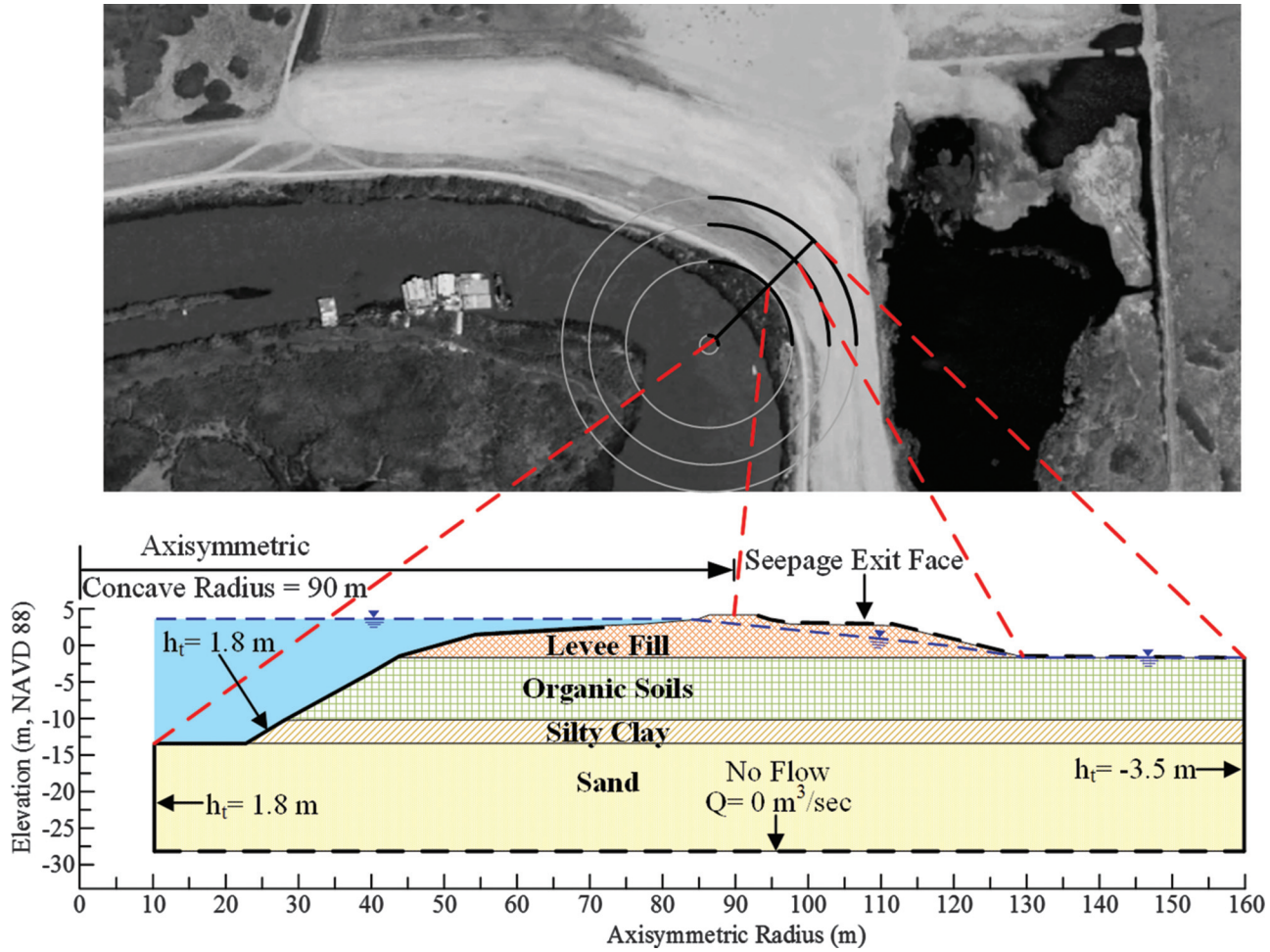

Fig. 2 in terms of an axisymmetric formulation. The axis of rotation in Fig. 15 is located at the origin or r = 0 m, and the 2D model starts at r = 10 m. The axis of rotation is located on the floodside because of the concave bend. The axisymmetric radius, defined from levee centerline to model origin, is determined by specifying three points along the levee crest and the following graphical procedure:

1. Draw two chords through points 1 and 2 and points 2 and 3.
2. Draw a perpendicular line from the midpoint of each chord so they intersect. The point of intersection is the center and origin of the axisymmetric analysis, and the distance between the center and any of the points is the radius of the circle.

An axisymmetric radius of 90 m is computed between Stations 528 and 532 in Fig. 15. The concave curve at Station 528 is modeled in SEEP/W with the boundary conditions depicted in Fig. 15. The axisymmetric vertical gradient of 0.18 between Stations 528 and 532 is displayed in Fig. 9 and shows that the 3D model and axisymmetric analysis in SEEP/W are in close agreement at the point of maximum curvature. The axisymmetric model and MODFLOW gradients separate after Station 530 because the axisymmetric model assumes the levee section is a circle, but the levee section (see Fig. 15) is straightening and therefore gradients begin to increase to 2D plane strain condition.

An axisymmetric model is also developed for the levee meander parametric analysis because convex (converging) and concave (diverging) flow conditions are present. The axisymmetric boundary conditions and soil profile are applied in a similar manner as in Fig. 15. Various radii ranging from 100 to 10 000 m are conducted to compare axisymmetric results with the levee meander vertical gradients in Fig. 14. The circular dots in Fig. 14 represent the axisymmetric vertical gradients and are found to match the MODLFLOW parametric analysis. Because the meanders in Fig. 11 are reduced to a series of radii (using the node procedure), equivalent radii develop the same vertical gradients independent of ω. Therefore, the radius of curvature can be used in an axisymmetric analysis to evaluate vertical gradients at a levee bend.

Table 3 summarizes the 3D and 2D vertical gradients for the levee meander parametric analysis. The MODFLOW and axisymmetric vertical gradients are 0.64 at r = 100 m, and thus a factor of 2 greater than the 2D gradient of 0.32. As the radius approaches 1000 m, the normalized values approach 1.05. The concave 3D results show 2D gradients overpredict gradients by about 1.8 and similarly approach 2D gradients at r = 1000 m. Based on the specific soil properties and cross section modeled, Table 3 shows that 3D analyses via MODFLOW and (or) axisymmetric are necessary to capture 3D effects of levee underseepage that are missed with a 2D analysis.

Axisymmetric analyses can be used to develop a design chart similar to Fig. 14 and Table 3 for levee segments with consistent subsurface profiles, boundary conditions, and material properties. The design chart can provide an approximation of 3D gradients for a range of radii. The radius of the levee bend is determined by the graphical procedure using three points along the levee centerline. If 3D uplift pressures that may cause sand boils or heaving are predicted, the uplift pressures or vertical

Table 3. Comparison of 3D and 2D vertical gradients for convex and concave levee bends.

	Convex vertical gradient		Concave vertical gradient	
Radius (m)	Axisymmetric and MODFLOW	Normalized[a] (3D/2D)	Axisymmetric and MODFLOW	Normalized[a] (3D/2D)
100	0.64	2	0.18	0.55
150	0.48	1.5	0.22	0.7
300	0.39	1.2	0.27	0.85
500	0.36	1.1	0.29	0.9
1000	0.34	1.05	0.31	0.95

[a]2D vertical gradient, 0.32.

gradients also can be used as input for design of remedial measures, such as relief wells, seepage berms, and cutoff walls.

Summary and conclusions

The state of practice to examine levee and floodwall seepage performance includes 2D plane strain FEA and analytical equations proposed in the USACE design manuals EM 1110-2-1901 and EM 1110-2-1913 (USACE 1993, 2000). The Sherman Island levee system is used to develop a calibrated seepage model and evaluate the effect of finite landside excavations and levee curvature on landside seepage results. This study shows that 2D analyses underpredict hydraulic gradients for convex levee bends and landside excavations with aspect ratios less than 1*L*:1.5*W*. The following observations and recommendations were derived from the 3D seepage analyses.

1. For the specific case of Sherman Island, a 3D analysis is required for a landside excavation with aspect ratios less than or equal to 1*L*:1.5*W*. The parametric analysis shows that narrow landside excavations, e.g., trenches, pipelines, conduits, animal burrows, and tree stumps–trunks, are important because vertical gradients rapidly increase below widths of 5 m. For cases such as drainage canals and ditches that parallel the levee toe and are greater than 20 m wide, the gradients at the center of the excavation are essentially equal to 2D vertical gradients. The critical location at a finite width excavation occurs near the edge of the excavation because of seepage inflow from the sidewalls.
2. The 3D MODFLOW model of Sherman Island levee shows concave levee bends diverge seepage, leading to lower vertical hydraulic gradients compared to 2D plane strain seepage models. The analyses also show convex bends, e.g., near Station 525, yield gradients greater than 2D values while the vertical gradients approach the 2D value when the levee is straight (close proximity to Station 535).
3. The pattern of levee curvature is defined herein using the SGC developed by Langbein and Leopold (1966), which can be used to describe river channels. Sine-generated curves are defined by a circular arc in the bend portion and transition from a circle at the apex to a straight segment at the point of inflection. By varying ω from 45° to 100°, the field-calibrated parametric analyses indicate sharper convex bends ($\omega = 100°$) cause vertical gradients that are about 150% greater than a 2D seepage model. Concave bends yield similar gradients for all values of ω because seepage is diverging in many directions away from the landside toe. When a segment of a levee bend is defined in terms of a radius, the vertical gradients compared to a 3D seepage model are approximately equal. Radial flow depends on the radius; hence, equivalent radii produce equivalent gradients.
4. Axisymmetric seepage models can be used to evaluate 3D vertical hydraulic gradients for convex levee bends. Although levee geometry can be irregular, a circular arc can approximate the maximum curvature by defining a three-point circle for a levee bend. The three-point circle graphical procedure can be used to identify the center and radius of a circle. The axisymmetric radius along with a 2D plane strain subsurface profile, material properties, and boundary conditions can be used in an axisymmetric seepage model to estimate 3D vertical gradients.

Acknowledgements

The authors thank Emily MacDonald of Wagner & Bonsignore for sharing Sherman Island piezometer data. This material is based upon work supported by the National Science Foundation through a Graduate Research Fellowship to Navid H. Jafari. Any opinions, findings, and conclusions or recommendations expressed in this material are those of the authors and do not necessarily reflect the views of the NSF, USACE, USDOJ, or any other agency or individual.

References

Ahmed, A., and Bazaraa, A. 2009. Three-dimensional analysis of seepage below and around hydraulic structures. Journal of Hydrology Engineering, ASCE, **14**(3): 243–247. doi:10.1061/(ASCE)1084-0699(2009)14:3(243).

American Standards and Test Methods (ASTM). 2011. Standard practice for classification of soils for engineering purposes (Unified Soil Classification System). ASTM standard D2487. American Society for Testing and Materials, West Conshohocken, Pa.

American Standards and Test Methods (ASTM). 2013. Standard Classification of Peat Samples by Laboratory Testing (D4427). *In* 2013 Annual Book of ASTM Standards, Volume 04.08. American Society for Testing and Materials, Philadelphia. doi:10.1520/D4427.

American Standards and Test Methods (ASTM). 2014. Standard Test Methods for Moisture, Ash, and Organic Matter of Peat and Other Organic Soils (D2974). *In* 2014 Annual Book of ASTM Standards, Volume 04.08. American Society for Testing and Materials, Philadelphia. doi:10.1520/D2974-14.

Benjasupattananan, S., and Meehan, C.L. 2012. Deterministic and probabilistic approaches for two- and three-dimensional levee underseepage analyses. *In* Proceedings Dam Safety 2012, ASDSO, Denver, CO, pp. 1–21.

Bennett, G.D., Reilly, T.E., and Hill, M.C. 1990. Technical training notes in ground-water hydrology: Radial flow to a well. U.S. Geological Survey, Water Resources Investigations Report 89-4134.

CALFED (CALFED) Bay Delta Program. 2000. Levee system integrity program plan, Final Programmatic EIS/EIR Technical Appendix.

California Department of Water Resources (DWR). 2005. Flood warnings: Responding to California's flood crisis, Resources Agency of California.

Cobos-Roa, D., and Bea, R. 2008. Three-dimensional seepage effects at three New Orleans levee breaches during Hurricane Katrina. Electronic Journal of Geotechnical Engineering, **13**(Bund. K): 1–26.

Connor, J.J., and Brebbia, C.A. 1976. Finite element techniques for fluid flow, Newnes-Butterworths, Boston, MA.

Coons, T., Soulard, C., and Knowles, N. 2008. High-resolution digital terrain models of the Sacramento/San Joaquin Delta region, California. USGS Data Series, **359**: 1–12. Available from http://pubs.usgs.gov/ds/359/.

Du, R. and Merry, S.M. 2014. The effect of the waterside boundary condition on the seepage and slope stability analyses of the Natomas Levees – A case study. *In* Proceedings of the GeoCongress 2014, Atlanta, GA, February 23–36, ASCE Geotechnical Special Publication 234, pp. 1511–1524.

Foott, R., Sisson, R., and Bell, R. 1992. Threatened Levees on Sherman Island. *In* Proceedings Stability and Performance of Slopes and Embankments II, ASCE, Berkeley, California, pp. 756–774.

Geo-Slope. 2007. Slope/W software Users Guide. Geo-Slope International Ltd., Calgary, Canada.

Hanson, J.C. (Hanson) Consulting Civil Engineer. 2009. Reclamation District 341 Sherman Island five-year plan, SH 08-3.0. California DWR, Sacramento, CA.

Harbaugh, A.W. 2005. MODFLOW-2005, The U.S. Geological Survey modular ground-water model—the ground-water flow process, USGS Techniques and Methods 6-A16.

Langbein, W.B., and Leopold, L.B. 1966. River meanders – Theory of minimum variance, physiographic and hydraulic studies of rivers, U.S. Geological Survey Professional Paper 422- H, H1-H15.

Merry, S.M., and Du, R. 2015. Plane strain versus axisymmetric modeling of convex levees. accepted for publication. Journal of Geotechnical and Geoenvironmental Engineering, ASCE, **141**(4): 04014121. doi:10.1061/(ASCE)GT.1943-5606.0001255.

Mesri, G., and Ajlouni, M. 2007. Engineering properties of fibrous peats. Journal of Geotechnical and Geoenvironmental Engineering, ASCE, **133**(7): 850–866. doi:10.1061/(ASCE)1090-0241(2007)133:7(850).

Mesri, G., Stark, T.D., Chen, C.S., and Ajlouni, M. 1997. Secondary compression of peats with and without surcharging. Journal of Geotechnical and Geoenvironmental Engineering, ASCE, **123**(5): 411–421. doi:10.1061/(ASCE)1090-0241(1997)123:5(411).

Money, R. 2006. Comparison of 2D and 3D seepage model results for excavation near levee toe. *In* Proceedings Geo-Congress 2006: Geotechnical Engineering

in the Information Technology Age, Atlanta, GA, 26–28 February 2006, American Society of Civil Engineers, 1–4.
Morisawa, M. 1985. Rivers: Form and process, Geomorphology Texts, Longman, New York.
Prokopovitch, N.P. 1985. Subsidence of peat in California and Florida. Environmental & Engineering Geoscience, **22**(4): 395–420. doi:10.2113/gseegeosci.xxii.4.395.
Rao, S.S. 1999. The finite element method in engineering, 3rd ed. Butterworths-Heinemann, Boston, MA.
Reddy, J.N. 1993. An introduction to the finite element method, 2nd Ed., McGraw-Hill, Hightstown, NJ.
Rocscience. 2014. RS^3 User's Guide. Rocscience Inc. Toronto, Canada.
Shelmon, R.J., and Begg, E. 1975. Late quaternary evolution of the Sacramento-San Joaquin Delta, California. *In* Quaternary Studies Bulletin, **13**. *Edited by* R.P. Suggate and M.M. Creswell. Wellington, NZ, pp. 259–266.
Soar, P.J., and Thorne, C.R. 2001. Channel restoration design for meandering rivers, ERDC/CHL Report CR-01-1, USACE Engineer Research and Development Center, Vicksburg, Mississippi.
Stark, T.D., and Jafari, N.H. 2015. Ruling on IHNC floodwall failures during Hurricane Katrina. Journal of Legal Affairs and Dispute Resolution, ASCE, **7**(3): 06715001. doi:10.1061/(ASCE)LA.1943-4170.0000167.
URS. 2013. Guidance document for geotechnical analyses, DWR Urban levees evaluations project, Version 13, Sacramento, CA.
U.S. Army Corps of Engineers. (USACE). 1993. Seepage analysis and control for dams. EM 1110-2-1901, Department of the Army, Washington, D.C.
USACE. 2000. Engineering and design—design and construction of levees. EM 1110-2-1913, Department of the Army, Washington, D.C.
USDA. 2014. Geospatial Data Gateway. Available from http://datagateway.nrcs.usda.gov/GDGHome.aspx [accessed 18 October 2013].
Washington Group International (WGI). 2005. Post-NFAATT groundwater characterization report, Inner Harbor Navigation Canal, East Bank Industrial Area. Washington Group International, Inc.
Weber, W.G. 1969. Performance of embankments constructed over peat. Journal of the Soil Mechanics and Foundations Division, ASCE, **95**(SM1): 53–76.
Yalin, M.S. 1992. River mechanics, Pergamon Press, Oxford.